The effects of visuospatial attention measured across visual cortex using source-imaged, steady-state EEG

Supplementary experimental procedures

Eye tracking

Although all our subjects were experienced psychophysical observers who were practiced in our task and our stimuli were well separated from the central fixation point, eye movements were a potential confound in this study. We tested the stability of eye fixation for seven of our subjects in separate sessions. Subjects performed an identical task to that used in the EEG experiments while their eye position was monitored with an Eyelink 1000 (SR Research, Chicago, IL) eye tracker sampling at 250 Hz. Viewing was binocular, but only the dominant eye of each subject was tracked. Head position was maintained with a chin rest. Calibration under these conditions is very stable, with high precision and very little drift over the course of an experiment (30–40 arc minutes in our case). Calibration was performed in two stages. First, observers viewed a static cross that was made of 0.1° dots placed centrally, ±5° vertically, and ±5° and ±10° horizontally. Observers were instructed to view each dot in turn as the eye tracker was manually adjusted to return a linear readout in response to eye position. Next, observers fixated a dynamic 0.25° dot that blinked on for 1500 ms and swept out a 5 × 5 calibration grid that covered the stimulus space in steps of 5° horizontally and 3.5° vertically. This grid was used to apply a perspective transformation to the raw eye position data, correcting any non-linearity that may occur near the edges of the display. The nominal standard deviation of this system's measurements is 0.25°, and we have confirmed this in separate experiments. At the end of the eye tracking experiment, we repeated the second part of the calibration to verify that it was within the nominal standard deviation (Supplementary Figures 1 and 2).

Given the size of the fixation point and the precision of the eye tracking system, we found that an ideal observer would maintain fixation within 0.5° 83.9% of the time and 1° 99.6% of the time if they fixated exactly at the edge of the fixation point. All subjects maintained fixation within 0.5° for an average of 86.5% of the time and within 1° for an average of 99.2% of the time (Supplementary Figure 3, Supplementary Table 1). Both measures indicate that the subjects were able to perform the covert attention task while maintaining fixation on the fix point. Further, the average frequency of saccades ending in the attended grating was 0.48/min during the attention trials, with no more than one saccade for any single 15-s trial.

Crosstalk estimation of source-imaged SSVEPs

Experimental procedures

Because the spatial resolution of our imaging technique is limited, the CCD estimate for a given ROI may be contaminated by signals from the surrounding cortical areas. To estimate the amount of "crosstalk" in a given ROI, we modeled the contribution from each visual cortical area to the other visual areas using the electrical head models that formed the basis of our source imaging computation (Lin et al., 2006; Liu, Dale, & Belliveau, 2002). Briefly, we simulated periodic signals in single cortical areas and used our electrical forward model to calculate the resulting voltage distribution on the scalp. Forward model simulations of this type are highly over-constrained and result in a single scalp voltage distribution for each active ROI. We then applied the identical source imaging procedures used on the measured data to these simulated "sensor space" data, computing the minimum norm cortical current density. In effect, we asked "given a true signal isolated to a single region, how much crosstalk are we likely to see in other, unstimulated locations?".

Results and discussion

Source imaging of high-density EEG recordings allows us to estimate the current density at different, well-defined cortical locations in individual subjects. The spatial error of source imaging methods such as the ones applied in this study has been reported to be 10–20 mm using 30 to 70 electrodes (Bai, Towle, He, & He, 2007; Im et al., 2007; Liu et al., 2002; Sharon, Hämäläinen, Tootell, Halgren, & Belliveau, 2007) and this number will decrease slightly with higher electrode density (128 in this study). Given that the Euclidean distance between the cortical areas studied here is at least 2 cm, we are confident that we can resolve independent responses in the areas that we have chosen. This is confirmed by differences in the response properties in the different areas. The contrast response

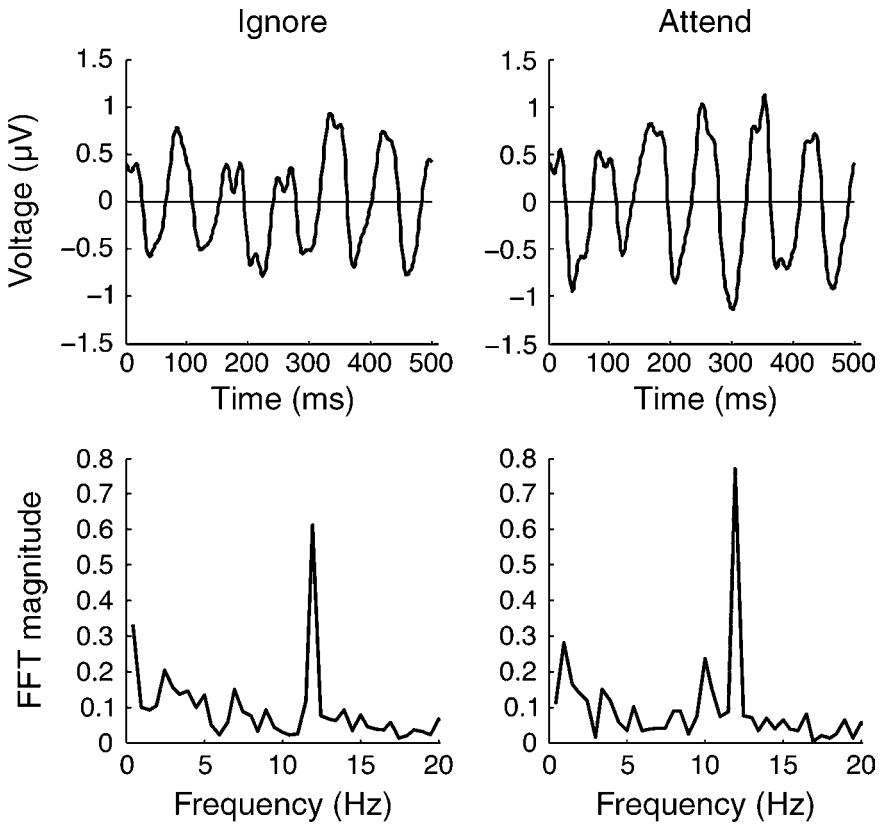

Supplementary Figure 1. Sample SSVEP traces for a single subject from a single electrode (electrode 64) over the left occipital cortex. The electrode is contralateral to a 12-Hz grating stimulus at 50% contrast. The 12-Hz oscillation is easily observed both when the right grating is ignored (the subject is attending the left grating) and when the grating is attended, and the amplitude appears higher in the attend condition. The Fourier transform of the SSVEP traces reveals a 12-Hz component that is significantly larger than background and is larger for the attend than ignore condition.

function is different for the four areas (Figure 4, gray lines), and in particular, we see far earlier saturation in area hMT+ compared to area V1. This smaller semi-saturation constant is a well-documented feature of the population responses in area hMT+ and the macaque homologue MT and has been measured previously using both single units (Sclar, Maunsell, & Lennie, 1990) and fMRI (Tootell et al., 1995). In addition, there is no evidence that areas close in distance have more similar contrast response functions.

The resolution and accuracy of source-imaged EEG and MEG is a topic of considerable debate. Although some

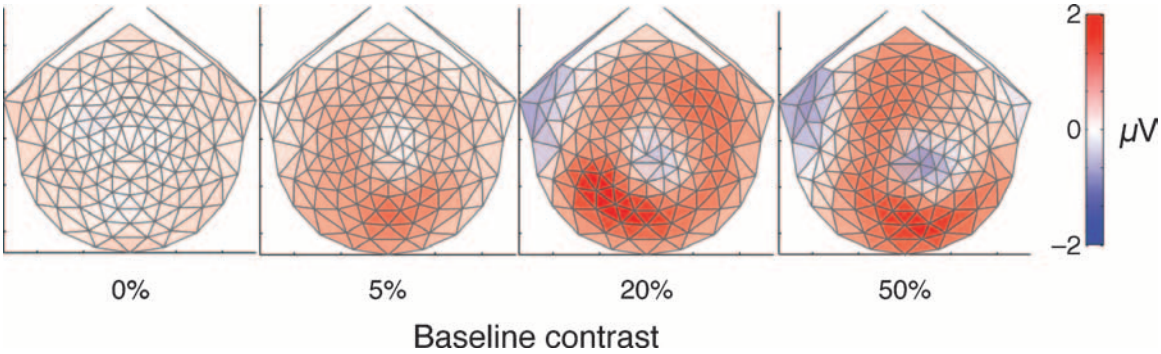

Supplementary Figure 2. Topographic maps of response amplitude *differences* (attended − ignored) averaged across observers (N = 15) and temporal frequencies (F1 and F2), i.e., (F1 attend left + F2 attend right) − (F1 attend right + F2 attend left). Maps are in a standard orientation with the anterior electrodes at the top and the reference electrode in the center. Much of the detailed spatial information that is preserved in the cortical ROI-based analysis (see main paper) is lost in this representation, but the overall trend, an increasing difference with baseline contrast and a concentration of signal over occipital cortex, is clear.

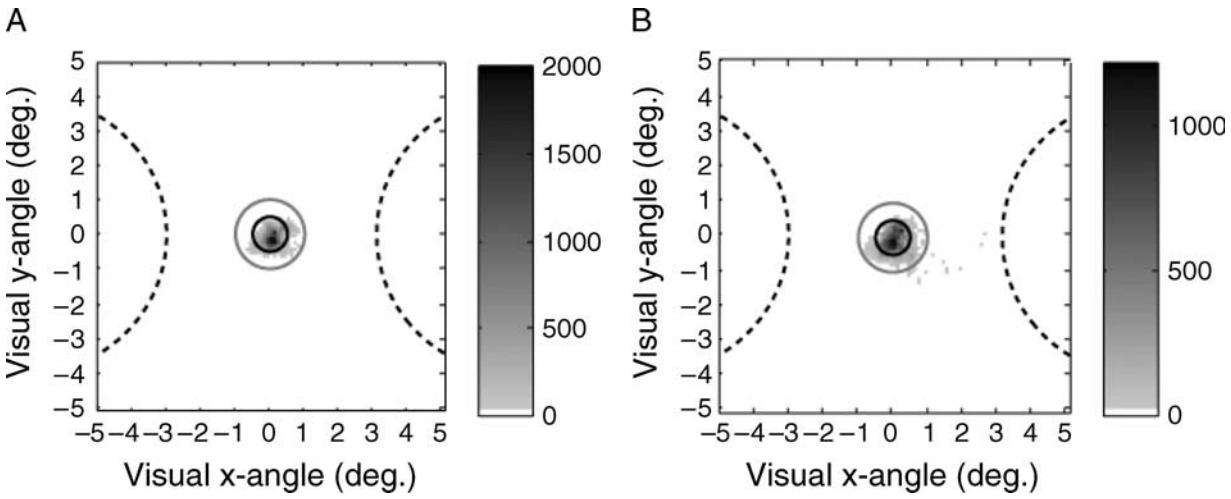

Supplementary Figure 3. Eye tracker data for subject 1. (A) Attend left. (B) Attend right. Grayscale indicates histogram values at different *x* and *y* eye positions in 0.1° bins of visual angle. The dashed rings indicate the location of the stimulus gratings, the solid black ring indicates a radius of 0.5°, and the solid gray ring indicates a radius of 1° of visual angle used as a measure of fixation in Supplementary Table 1. Note that the *x* and *y* positions have a similar spread, and that the *x* positions in (A) and (B) are not skewed in the left and right directions. Both indicate that the subject did not move eye position toward the location of the attended grating.

groups (Bai et al., 2007; Sharon et al., 2007) have reported remarkably high resolution, these studies have used additional constraints (for example, imaging the very earliest cortical responses) and/or combinations of imaging methodologies slightly different to our own to identify the locations of very specific signal components. Without these constraints, we believe that the estimate of a 2-cm resolution on the cortex from other studies in the literature is reasonable, and below, we describe an attempt to quantify the resolution of our technique more precisely.

To the amount of "crosstalk error" in the cortical current density estimation, we calculated what the contribution to the estimated cortical current density in each cortical area would be from neural activity within that area compared to crosstalk from neural activity in other visual areas including V2, V3, V3A, and lateral occipital cortex (LOC). As shown in Supplementary Figure 4, the crosstalk contribution from neighboring regions is relatively small. Since the estimated attention modulation is the same order of magnitude for the different areas, it cannot be explained solely by crosstalk estimation errors in any of the studied areas, including V1. This method cannot account for potential systematic localization biases due to errors in our electrical models. However, the fact that our data are robust when averaged across observers with different cortical sizes, geometries, and skull thicknesses argues against this possibility. Finally, our crosstalk estimates between V1, V2, and V3 are similar to those estimated by Hagler et al. (2009) modeling the minimum norm estimate on a much smaller number (3, 48, or 144) of current sources.

This observation is particularly important for the conclusions that V1 displays attentional modulation. Both V2 and V3 lie close to V1 and share a common foveal representation. Even V3A, with a separate foveal representation (Press, Brewer, Dougherty, Wade, & Wandell,

	Attend left					Attend right				
Subject	*SD*(*x*)	*SD*(*y*)	% < 0.5°(*x*)	% < 1°(*x*)	Sacc. end in grating/min	*SD*(*x*)	*SD*(*y*)	% < 0.5°(*x*)	% < 1°(*x*)	Sacc. end in grating/min
1	0.45	0.39	92.3	99.7	0.27	0.39	0.34	90.5	99.8	0.53
2	0.38	0.29	93.0	98.3	1.07	0.34	0.25	90.4	99.3	0.27
3	0.48	0.48	77.2	98.0	0.27	0.71	0.59	67.2	99.5	0.27
4	0.39	0.27	94.0	99.2	0.53	0.44	0.36	92.6	99.6	1.07
5	0.23	0.24	97.4	100	0.00	0.34	0.23	88.6	100	0.00
6	0.49	0.49	86.2	99.4	0.80	0.46	0.46	89.8	99.6	0.27
7	0.52	0.34	81.4	96.8	0.53	0.76	0.44	70.9	99.8	0.80
Pop. avg.	0.42	0.34	88.8	98.8	0.50	0.50	0.38	84.3	99.6	0.46

Supplementary Table 1. Eye tracking results. Standard deviation in the *x* and *y* coordinates of the eye position in degrees, the time the subject was within 0.5° and 1° of fixation in the *x* coordinate, and the frequency of saccades per minute ending within the attended grating.

2001; Smith, Greenlee, Singh, Kraemer, & Hennig, 1998; Tootell et al., 1997), is located close enough in Euclidian space to V1 to lead to some potential crosstalk from this area. Since the crosstalk from different areas are vectors, they do not sum linearly, but it is possible to determine an upper bound or "worst case" for the total crosstalk using their arithmetic sum. From Figure 9, the crosstalk terms to left V1 (LV1) from LV2 and LV3 are 0.19 and 0.22 in normalized units, respectively, and so the upper bound of their contribution to LV1 is 0.41, or (0.41/(1 + 0.41) =) 29.1% compared to the estimated density arising from LV1 itself. Similarly, the upper bound of the crosstalk to right V1 (RV1) from RV2/RV3 is 28.6%. The inter-hemispheric contribution is 27.3% from RV2/RV3 to LV1 and 25.4% from LV2/LV3 to RV1, so the difference between intra- and inter-hemispheric crosstalk is 2.5%. Given the task design, these differences influence the attend versus ignore differences of the V1 cortical current density estimate.

We believe, therefore, that attentional modulation in the CCD time course estimate from V1 is dominated by neural activity originating in the striate cortex. If this were not the case, the estimated attention increase in the V1 cortical current estimate would have to arise predominantly from areas V2 and V3. This is not, in itself, unreasonable, but given the weakness of the difference between the intra- and inter-hemispheric crosstalk from these areas to V1, the modulation in V2/V3 would have to be at least 40 times higher than the estimated V1 increase. We see no sign of an attentional modulation of this magnitude in any other areas. Given that the estimated attention modulations in hV4, hMT+, and IPS are similar to those in V1 (Figure 4), it seems clear that the predominant part of the attention increase in our V1 estimate must be due to changes in V1 neural activity. Similarly, if V3A is included in this type of estimation, the upper bound of the crosstalk estimate is 13.2%, requiring the attention increase in V2/V3/V3A to be at least ~8 times than the

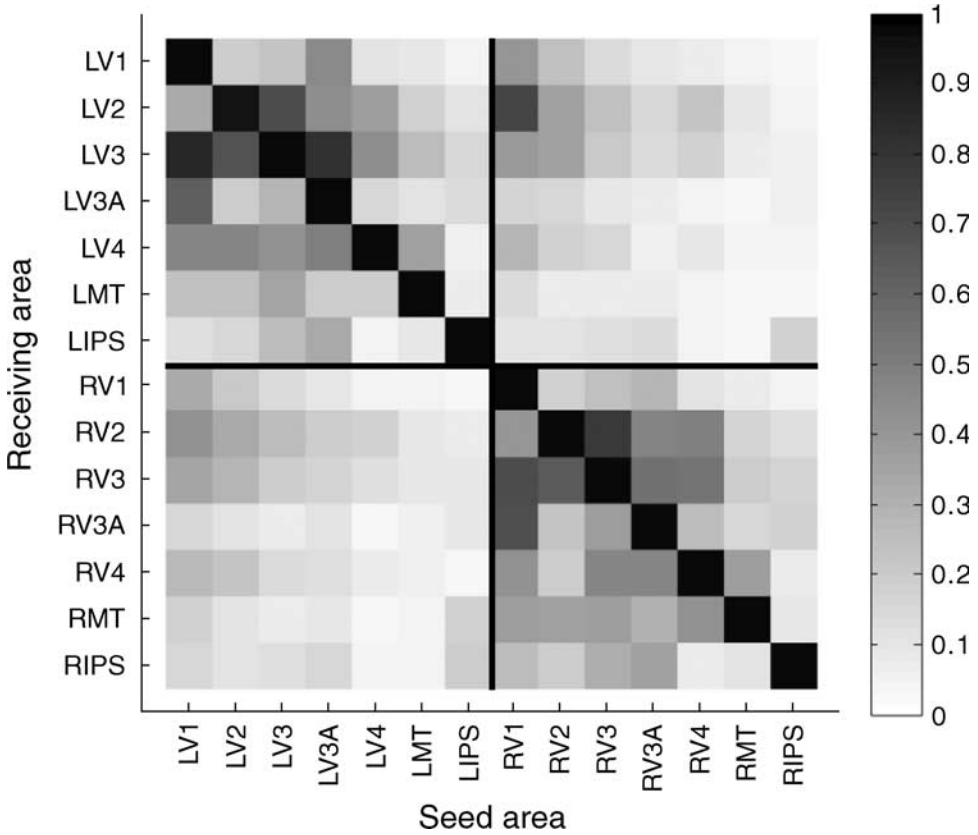

Supplementary Figure 4. Theoretical estimates of crosstalk between source-imaged EEG signals in retinotopically defined visual areas. Grayscale values at row i and column j represent the relative contribution of area j to the cortical current density estimate in area i. Individual left and right hemisphere definitions of the four studied areas (V1, hV4, hMT+, IPS) as well as V2, V3, V3A, and LOC are included. Thick lines are added to ease separation into left and right hemispheres. For each area, we modeled how its actual current influenced the estimated cortical current density in all areas. Zero crosstalk would correspond to a matrix with zeros off the main diagonal. We measure weak but significant crosstalk between some neighboring areas (for example, left V3A has some input to left V1). Crosstalk is mainly seen within hemispheres and between areas in close physical proximity. Overall, the crosstalk to V1 is relatively small: no other area contributes more than 37% of the signal compared to this area per unit cortical area. Since V1 is the one of the largest unitary areas in the visual cortex, the estimated V1 responses we report here are likely to be driven predominantly by V1 itself.

observed increase in V1. This is still much higher than the attention modulation we observe in any other area.

The simulations above indicate that most of the signals coming from the regions we term "V1," "hV4," "hMT+," and "IPS" should, in fact, derive from those retinotopically defined ROIs. However, we also acknowledge that there are significant contributions from neighboring regions and that there must also be some additional loss of resolution due to factors that we do not simulate such as imprecision in digitizing the locations of scalp electrodes, uncertainty about the conductivity of the different brain compartments, and the finite resolution of our boundary element models. In all likelihood therefore, our data represent estimates of neural responses in cortical regions centered on these ROIs but encompassing some of the surrounding visual area "cluster" (Wandell, Brewer, & Dougherty, 2005; Wandell, Dumoulin, & Brewer, 2007). Clusters appear to be a fundamental organizing feature of the visual cortex: regions with independent retinotopic maps but similar functional properties are arranged in a "pinwheel" fashion around a common foveal representation. The ROIs that we analyze in this paper all lie within, or close to, separate clusters. The "MT" cluster, for example (there is currently no standardized nomenclature), contains a group of areas thought to be involved in motion perception (Kolster, Peeters, & Orban, 2010). The "V1" cluster contains a group of early retinotopic visual areas sharing a common foveal representation at the posterior end of the calcarine sulcus and both the IPS ROI and hV4 ROI lie close to independent dorsal- and ventral-surface foveal representations, respectively (Brewer, Liu, Wade, & Wandell, 2005; Press et al., 2001; Swisher, Halko, Merabet, McMains, & Somers, 2007; Wade, Brewer, Rieger, & Wandell, 2002). We therefore consider it reasonable to assign the responses we describe in this paper to clusters of closely related areas rather than isolated retinotopic maps and the fundamental conclusions of our paper are not significantly weakened by this generalization. We consider the responses from the V1 ROI to be a somewhat special case. V1 is a relatively large area (Dougherty et al., 2003) extending onto the posterior lateral surface of the occipital cortex and strongly constrained by cortical folding patterns. Activity in V1 generates strong scalp responses, and contrary to earlier reports, V1 responses to stimuli in upper and lower visual hemifields do not cancel (Ales, Carney, & Klein, 2010; Ales, Yates, & Norcia, 2010) although they do in neighboring area V2. Because of these factors, we believe that the majority of the signals that we assign to this ROI do, in fact, arise in the striate cortex and not in adjacent areas V2 and V3.

References

Ales, J. M., Carney, T., & Klein, S. A. (2010). The folding fingerprint of visual cortex reveals the timing of human V1 and V2. *Neuroimage, 49,* 2494–2502.

Ales, J. M., Yates, J. L., & Norcia, A. M. (2010). V1 is not uniquely identified by polarity reversals of responses to upper and lower visual field stimuli. *Neuroimage, 52,* 1401–1409.

Bai, X., Towle, V. L., He, E. J., & He, B. (2007). Evaluation of cortical current density imaging methods using intracranial electrocorticograms and functional MRI. *Neuroimage, 35,* 598–608.

Brewer, A. A., Liu, J., Wade, A. R., & Wandell, B. A. (2005). Visual field maps and stimulus selectivity in human ventral occipital cortex. *Nature Neuroscience, 8,* 1102–1109.

Dougherty, R. F., Koch, V. M., Brewer, A. A., Fischer, B., Modersitzki, J., & Wandell, B. A. (2003). Visual field representations and locations of visual areas V1/2/3 in human visual cortex. *Journal of Vision, 3*(10):1, 586–598, http://www.journalofvision.org/content/3/10/1/, doi:10.1167/3.10.1. [PubMed] [Article]

Hagler, D. J., Jr., Halgren, E., Martinez, A., Huang, M., Hillyard, S. A., & Dale, A. M. (2009). Source estimates for MEG/EEG visual evoked responses constrained by multiple retinotopically-mapped stimulus locations. *Human Brain Mapping, 30,* 1290–1309.

Kastner, S., De Weerd, P., Desimone, R., & Ungerleider, L. G. (1998). Mechanisms of directed attention in the human extrastriate cortex as revealed by functional MRI. *Science, 282,* 108–111.

Kolster, H., Peeters, R., & Orban, G. A. (2010). The retinotopic organization of the human middle temporal area MT/V5 and its cortical neighbors. *Journal of Neuroscience, 30,* 9801–9820.

Lin, F.-H., Witzel, T., Ahlfors, S. P., Stufflebeam, S. M., Belliveau, J. W., & Hämäläinen, M. S. (2006). Assessing and improving the spatial accuracy in MEG source localization by depth-weighted minimum-norm estimates. *Neuroimage, 31,* 160–171.

Liu, A. K., Dale, A. M., & Belliveau, J. W. (2002). Monte Carlo simulation studies of EEG and MEG localization accuracy. *Human Brain Mapping, 16,* 47–62.

Press, W. A., Brewer, A. A., Dougherty, R. F., Wade, A. R., & Wandell, B. A. (2001). Visual areas and spatial summation in human visual cortex. *Vision Research, 41,* 1321–1332.

Sclar, G., Maunsell, J. H. R., & Lennie, P. (1990). Coding of image contrast in central visual pathways of the macaque monkey. *Vision Research, 30,* 1–10.

Sharon, D., Hämäläinen, M. S., Tootell, R. B., Halgren, E., & Belliveau, J. W. (2007). The advantage of combining MEG and EEG: Comparison to fMRI in focally stimulated visual cortex. *Neuroimage, 36,* 1225–1235.

Smith, A. T., Greenlee, M. W., Singh, K. D., Kraemer, F. M., & Hennig, J. (1998). The processing of first- and

second-order motion in human visual cortex assessed by functional magnetic resonance imaging (fMRI). *Journal of Neuroscience, 18,* 3816–3830.

Swisher, J. D., Halko, M. A., Merabet, L. B., McMains, S. A., & Somers, D. C. (2007). Visual topography of human intraparietal sulcus. *Journal of Neuroscience, 27,* 5326–5337.

Tootell, R. B., Hadjikhani, N., Hall, E. K., Marrett, S., Vanduffel, W., Vaughan, J. T., et al. (1998). The retinotopy of visual spatial attention. *Neuron, 21,* 1409–1422.

Tootell, R. B., Mendola, J. D., Hadjikhani, N. K., Ledden, P. J., Liu, A. K., Reppas, J. B., et al. (1997). *Functional analysis of V3A and related areas in human visual cortex* (vol. 17).

Tootell, R. B. H., Reppas, J. B., Kwong, K. K., Malach, R., Born, R. T., Brady, T. J., et al. (1995). Functional analysis of human MT and related visual cortical areas using magnetic resonance imaging. *Journal of Neuroscience, 15,* 3215–3230.

Wade, A. R., Brewer, A. A., Rieger, J. W., & Wandell, B. A. (2002). Functional measurements of human ventral occipital cortex: Retinotopy and colour. *Philosophical Transactions of the Royal Society of London B: Biological Sciences, 357,* 963–973.

Wandell, B. A., Brewer, A. A., & Dougherty, R. F. (2005). Visual field map clusters in human cortex. *Philosophical Transactions of the Royal Society of London B: Biological Sciences, 360,* 693–707.

Wandell, B. A., Dumoulin, S. O., & Brewer, A. A. (2007). Visual field maps in human cortex. *Neuron, 56,* 366–383.